Faculty and Student Publications   Engineering, School of

10-1-2020

A mathematical framework for estimating risk of airborne transmission of COVID-19 with application to face mask use and social distancing

Rajat Mittal
Johns Hopkins University

Charles Meneveau
Johns Hopkins University

Wen Wu
University of Mississippi

Recommended Citation

A mathematical framework for estimating risk of airborne transmission of COVID-19 with application to face mask use and social distancing 🅕

🆔 Rajat Mittal, 🆔 Charles Meneveau, and 🆔 Wen Wu (武文)

COLLECTIONS

Paper published as part of the special topic on Flow and the Virus

🅕   This paper was selected as Featured

View Online   Export Citation   CrossMark

ARTICLES YOU MAY BE INTERESTED IN

Aerosol persistence in relation to possible transmission of SARS-CoV-2
Physics of Fluids **32**, 107108 (2020); https://doi.org/10.1063/5.0027844

Numerical investigation of aerosol transport in a classroom with relevance to COVID-19
Physics of Fluids **32**, 103311 (2020); https://doi.org/10.1063/5.0029118

Dispersion of evaporating cough droplets in tropical outdoor environment
Physics of Fluids **32**, 113301 (2020); https://doi.org/10.1063/5.0026360

A mathematical framework for estimating risk of airborne transmission of COVID-19 with application to face mask use and social distancing ⓕ
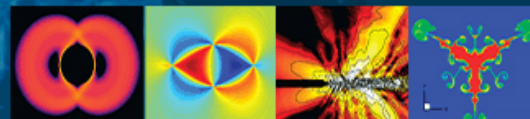
Rajat Mittal,[1,2,a] ⓘ Charles Meneveau,[1] ⓘ and Wen Wu (武文)[3] ⓘ

AFFILIATIONS

[1] Mechanical Engineering, Johns Hopkins University, 3400 N. Charles St., Baltimore, Maryland 21218, USA
[2] School of Medicine, Johns Hopkins University, 3400 N. Charles St., Baltimore, Maryland 21218, USA
[3] Mechanical Engineering, University of Mississippi, 209C Carrier Hall, Oxford, Mississippi 38677, USA

[a] Author to whom correspondence should be addressed: mittal@jhu.edu

ABSTRACT

A mathematical model for estimating the risk of airborne transmission of a respiratory infection such as COVID-19 is presented. The model employs basic concepts from fluid dynamics and incorporates the known scope of factors involved in the airborne transmission of such diseases. Simplicity in the mathematical form of the model is by design so that it can serve not only as a common basis for scientific inquiry across disciplinary boundaries but it can also be understandable by a broad audience outside science and academia. The caveats and limitations of the model are discussed in detail. The model is used to assess the protection from transmission afforded by face coverings made from a variety of fabrics. The reduction in the transmission risk associated with increased physical distance between the host and susceptible is also quantified by coupling the model with available and new large eddy simulation data on scalar dispersion in canonical flows. Finally, the effect of the level of physical activity (or exercise intensity) of the host and the susceptible in enhancing the transmission risk is also assessed.

Published under license by AIP Publishing. https://doi.org/10.1063/5.0025476

I. INTRODUCTION

COVID-19 has spread across the world with a speed and intensity that have laid bare the limits of our understanding of the transmission pathways and the associated factors that are key to the spread of such diseases. There is, however, an emerging consensus that "airborne transmission," where virion bearing respiratory droplets and droplet nuclei (also called respiratory aerosols) expelled by an infected person (the "host") are inhaled by a "susceptible" individual, constitutes an important mode for the spread of COVID-19.[1–5] Questions regarding the size of the droplets involved[6–9] and the range of such transmission[10] can be bypassed by noting that the key element that differentiates airborne transmission from the droplet and contact routes of transmission[11] is the essential role of *inhalation* by the susceptible in the pathway for transmission.

Generally, it is the small (<10 μm) particles that are likely to be entrained into the inhalation current of a person, while environmental conditions as well as the proximity between the host and the susceptible could allow larger particles/droplets to play a role in airborne transmission.

Irrespective of the size of droplets or the range involved, the airborne transmission of COVID-19 and other respiratory infections involve the following sequence of events (see Fig. 1):

1. generation, expulsion, and aerosolization of virus-containing droplets from the mouth and nose of an infected host,
2. dispersion and transport via ambient air currents of the respiratory aerosols to a susceptible, and
3. inhalation of droplets/aerosols and deposition of virus in the respiratory mucosa of the susceptible.
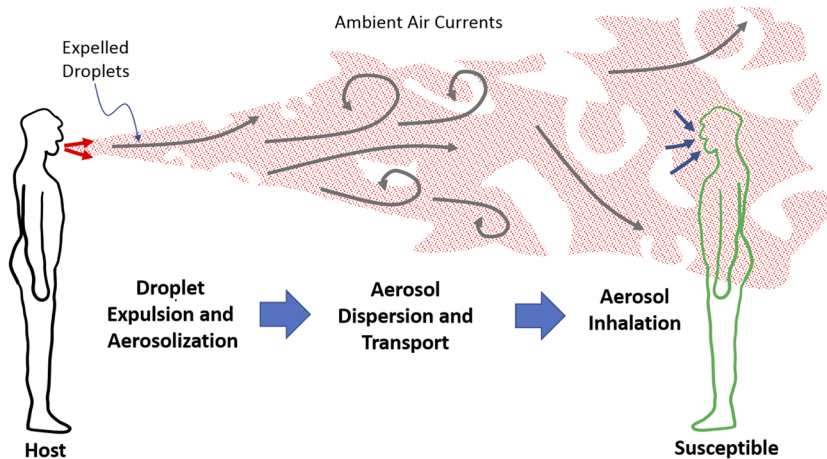
Each phase in this sequence has complex dependencies on a variety of factors that may include the morphological properties and pathogenicity of the virus, the health status of the host and/or the susceptible, environmental conditions, and the presence/effectiveness of face coverings being used by the host and/or susceptible. Given this complexity of phenomenology and the many factors involved, it is not surprising that even after more than eight months of the world dealing with the COVID-19 pandemic, there are fundamental questions that continue to confound scientists, policy makers, and the members of the public at large. These include the following questions: What factors have enabled the SARS-CoV-2 to spread so much faster and more extensively than other similar viruses in the recent past?[12,13] Why is the rate of infection so different in different regions/countries of the world?[14] How much lower is the likelihood of transmission in an outdoor environment compared to an indoor environment?[10,15] How do policies and societal behavior such as compliance with mask wearing affect the rate of transmission?[16,17] Finally, how does the transmission risk reduce with distance between the host and the susceptible?

Scientists spanning fields such as biomedicine, epidemiology, virology, public health, fluid dynamics, aerosol physics, public policy, behavioral psychology, and others are tackling these as well as other important questions. However, what is lacking is a simple and intuitive conceptual framework (or model) that encapsulates the complex, multifactorial scope of this problem in a manner that not only serves as a common basis for scientific inquiry across disciplinary boundaries but also as a tool to more easily communicate the factors associated with the spread of this disease to a wide range of stakeholders including non-scientists such as policy-makers, public media, and the public at large. Given the rapidly evolving nature of the pandemic and the resurgence of infections in many communities,[18] the importance of clear communication of infection risk across scientific disciplines, as well as to policy/decision makers and other segments of society, is more important than ever.

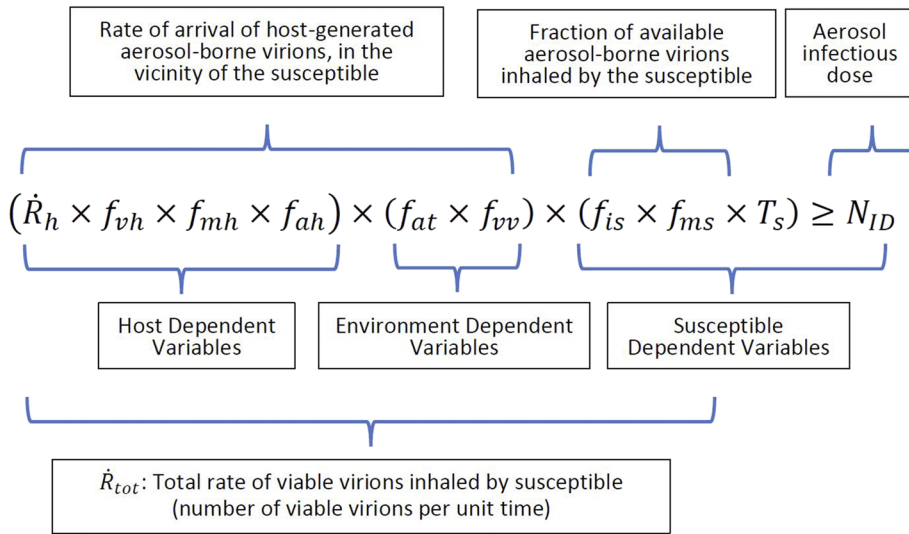## II. THE CONTAGION AIRBORNE TRANSMISSION (CAT) INEQUALITY

In 1961, Dr. Frank Drake, an astronomer and astrophysicist involved in the search for extraterrestrial intelligence, conceived a conceptual framework to predict the number of technological civilizations that may exist in our galaxy. The Drake equation,[19,20] as it has become known, involves a number of probabilistic factors, which when multiplied together result in the number of civilizations within our galaxy, at any given moment, that humanity could communicate with. The power of this equation is not in the fact that it actually allows us to predict this number with a known level of certainty, but in the fact that it provides an easy to understand framework for grasping the key factors involved in something that seems inestimable: the number of advanced life forms that exist elsewhere in our galaxy.

Motivated by the Drake equation, and based on the idea that airborne transmission occurs if a susceptible inhales a viral dose that exceeds the minimum infectious dose,[21,22] the model in Fig. 2 to predict the possibility of airborne transmission of a respiratory contagion such as SARS-CoV-2 from an infected host to a susceptible is proposed.

In the expression in Fig. 2, which we refer to as the Contagion Airborne Transmission (CAT) Inequality,

$\dot{R}_h$ represents the rate of expulsion of respiratory droplets from the nose and mouth of the host (number of droplets per unit time),

f_{vh} represents the fractional viral emission load—the average number of virions contained in each expelled droplet,

f_{mh} represents the fraction of expelled droplets that make it past the face covering of the host,

f_{ah} represents the fraction of expelled droplets that aerosolize (i.e., become suspended in the air),

f_{at} represents the fraction of aerosolized droplets that transport to the vicinity of the susceptible,

f_{vv} represents the fraction of aerosolized droplets transported to the vicinity of the susceptible that contain viable virions,

f_{is} represents the fraction of aerosols in the vicinity of the susceptible that would be inhaled by a susceptible not wearing a face covering,

f_{ms} represents the fraction of inhaled aerosols that are filtered by the face covering of the susceptible,

$\dot{R}_{tot}$ represents the total rate of viable virion inhalation by the susceptible (number per unit time),

FIG. 2. The contagion airborne transmission (CAT) inequality that evaluates the conditions for the airborne transmission of a respiratory infection such as COVID-19. The left-hand side of the inequality represents the total inhaled viral dose, and the right-hand side is the minimum aerosol dose required to initiate an infection in the susceptible. The inequality is satisfied (and the transmission is successful) when the susceptible inhales a viral dose that exceeds the minimum infectious dose. The variables in the model can be segregated in different ways, as shown in the graphic.

T_s represents the duration of exposure of the susceptible to the aerosols from the host, and

N_{ID} represents the minimum number of inhaled virions required to initiate an infection in the susceptible.

The CAT inequality is a mathematical model for the estimation of infection risk that can be used based on various interpretations of its constituent terms. For example, if $\dot{R}_{tot}$ and N_{ID} are known, then the CAT inequality allows one to deduce the critical exposure time $T_{sC} = N_{ID}/\dot{R}_{tot}$ below which an infection is unlikely. Most often in practice, however, not all of the factors in the inequality will be known. Still, the CAT inequality can be used to compare *relative* risks since one may consider the risk of a situation to be inversely proportional to the corresponding critical exposure time (e.g., halving the critical exposure time doubles the risk). For example, the risk ratio for two situations A and B will be $T_{sc-B}/T_{sc-A} = \dot{R}_{tot-A}/\dot{R}_{tot-B}$. Thus, if, e.g., all factors are equal for A and B except for one, e.g., $f_{mhA} \neq f_{mhB}$ (say), then the risk ratio comparing A to B will be f_{mhA}/f_{mhB}. In Sec. VIII, we will illustrate such relative risk estimations for three specific cases.

The use of mathematical models to predict infection rates is well established in epidemiology,[21,23,24] and the CAT inequality belongs among such models (see Sec. VIII for discussion on relationship to existing modeling frameworks). As with any model, the CAT inequality has a number of underlying assumptions (see Sec. IX), but its potential advantage is that it presents the transmission risk via a simple mathematical expression that, on one hand, captures a wide scope of factors that may be involved in airborne transmission and, on the other, is easy to convey to scientists from a wide range of fields, non-scientists such as policy makers, public officials, and public media, and even members of the general public.

As laid out in a previous publication,[11] each stage in the airborne transmission process is mediated by complex flow phenomena, ranging from air–mucous interaction and liquid sheet fragmentation inside the respiratory tract, to turbulence in the expiratory jet/ambient flow and flow-induced droplet evaporation and particle dispersion, to inhalation and deposition of aerosols in the lungs. Furthermore, non-pharmaceutical approaches employed to mitigate respiratory infections such as social distancing and wearing of face masks are also rooted in the principles of fluid dynamics. Thus, fluid dynamics is central to all important physical aspects of the airborne transmission of respiratory infections such as COVID-19, and it therefore stands to reason that this connection to flow physics will appear in any successful model of airborne transmission. In Secs. III–VI, we provide additional details about the key variables involved in the CAT inequality with special emphasis on the intervening fluid dynamical phenomena. This is followed by the application of the model to assess the transmission risk associated with face mask use, physical distancing, and exercise intensity in Sec. VII. Finally, Secs. IX and X, we describe the caveats associated with this model and summarize the study.

III. HOST RELATED VARIABLES

The CAT inequality (Fig. 2) naturally segregates into three sets of variables: the first set depends primarily on the host, the second depends on the environment, and the third depends on the susceptible. We now describe the factors that each of these variables depends on as well as our state of knowledge regarding each variable.

$\dot{R}_h$ is the rate of expulsion of respiratory droplets from the nose and mouth of the host and is one of the most extensively studied parameters within the arena of airborne transmission.[6,7,9,25–28] Droplets are formed from the mucus and saliva that line the respiratory and oropharyngeal tracts, and these droplets are expelled with the air that is exhaled out of the mouth and nose. Studies have shown that individuals generate more droplets for the same expiratory activity while ill with a respiratory infection than after recovery,[26,29] and this may be related to enhanced mucous production during illness. While the conventional notion is that sneezing has the highest rate of droplet generation followed by coughing,

talking,[7,30] and breathing[6] (in that order), the very large scatter in measured data[6,25,31] makes it difficult to validate this notion. Attention during the ongoing pandemic has focused on droplet generation during talking and breathing[7,8,25] due to the recognition that viral shedding from asymptomatic/presymptomatic individuals (who are not coughing or sneezing) may be an important differentiator in the high spreading rate of SARS-CoV-2 infections compared to earlier coronavirus outbreaks.[2,32]

For activities such as breathing and talking, it could be appropriate to express $\dot{R}_h$ as the product of the volume expiration (i.e., ventilation) rate of the host ($\dot{V}_{Eh}$) and the number density of droplets (i.e., droplets per unit volume) in the exhaled gas (n_{dh}). This is because for a given individual, n_{dh} might not vary significantly during activities such as breathing, and $\dot{R}_h$ would therefore increase linearly with the ventilation (i.e., exhalation) rate $\dot{V}_{Eh}$. The ventilation rate for an adult can range from about 100 ml s^{-1} at rest to 2000 ml s^{-1} during intense exercise.[33] The measured values of n_{dh} for breathing[34] are about 0.1 ml^{-1}, and this suggests that $\dot{R}_h$ for breathing could range from about 10 to 200 droplets per second depending on the ventilation rate. The values of n_{dh} during normal speech in the same experiment were found to be about two to eight times higher, and other studies have found that droplet emission increases with the loudness of speech.[7] Finally, recent attention has focused on "super producers": individuals who according to some studies generate droplets at rates that are 10 or more times higher than others.[29,35] Thus, even for normal breathing, $\dot{R}_h$ could range from about 10 s^{-1} to 2000 s^{-1} depending on the exhalation rate and the emission phenotype of the individual, and speech could increase the upper range by another order of magnitude. Thus, the phenotype and expiratory activity of the host alone could increase the transmission risk by a factor of 1000 or more.

f_{vh} is the fractional viral load of a respiratory droplet, i.e., the average number of virions per droplet, and there are currently no data on this variable for SARS-CoV-2. Indirect measures based on the volume concentration of viral load in oral fluid samples collected from COVID-19 patients combined with simple volumetric estimates have been used to suggest that 37% of 50 μm size droplets and 0.37% of 10 μm size droplets would contain virions.[30] No confirmation of these estimates from the direct measurement of respiratory aerosols is available so far, and there is evidence that suggests that these simple volume-fraction based estimates might significantly underestimate the viral load of the small (<5 μm) droplets.[27] Furthermore, the fractional viral load also likely depends on the location in the respiratory tract from where the droplet originates because pathogens tend to colonize specific regions of the respiratory tract and the mucous volume and thickness varies throughout the respiratory tract.[36] There is, however, no quantification of this effect. We note that employing even a low-end estimate of say a 0.5% fractional viral load (i.e., $f_{vh} = 0.005$), combined with 200 000 droplets/cough,[26] would result in the shedding of 1000 virions in each cough, and this could be equivalent to the minimum infectious dose (see the discussion in Sec. VI) for COVID-19.

f_{ah} is the fraction of expelled droplets that aerosolize, i.e., get suspended in the air. It is generally found that droplets smaller than about 10 μm can remain suspended in the air, whereas droplets larger than 50 μm fall to the ground rapidly.[34,37–39] Thus, the size distribution of the expelled droplets is a key determinant of f_{ah}. A number of studies have examined the distribution of droplet size

expelled during various expiratory activities,[6,7,9,25–28] and these studies show that the droplet size can vary from 0.01 μm to 1000 μm. The consensus is that breathing generates the smallest particles, while talking, coughing, and sneezing generate increasingly larger droplets (in that order).[40] There is however a large scatter in these data, and this might be due to subject-specific differences[41] as well as the changes in the mucosal fluid induced by the pathogen.[40] Finally, the fluid in the expelled droplets also evaporates rapidly, resulting in a reduction in the size, and this rate of evaporation may depend on prevailing conditions of temperature and humidity near the host, as well as the velocity of the droplets. These dependencies can, however, be determined, for the most part, from first principles.[38,42]

IV. ENVIRONMENT DEPENDENT VARIABLES

f_{at} represents the fraction of aerosolized respiratory aerosol droplets/droplet nuclei from the infected host that are transported to the immediate vicinity of the susceptible, and this is one variable where environmental factors play a dominant role. These include air currents, turbulence, temperature, and humidity. Ambient air currents in particular determine the "time-of-flight" as well as the dilution in the concentration of the bioaerosol that arrives near the susceptible.

Even though we know the dependencies of the variable f_{at}, it is still a difficult variable to estimate since environmental factors can be so highly variable.[43] The estimation of this parameter becomes particularly difficult in indoor spaces such as buildings where rooms share a high-volume air conditioning (HVAC) system. In high-density indoor spaces such as classrooms, aircraft cabins, gyms, buses, trains, and so on, anthropogenic effects generated due to human movement and body heat generated thermal plumes[46,47] could also have a significant effect on this variable. For example, even for a host and susceptible in the same room, this variable could change significantly given the relative location of the two individuals, the operational status of the air conditioning, and the location of the individuals relative to the air conditioning diffusers and vents.[15,44,45] The effects of indoor ventilation fluid dynamics on COVID-19 transmission have been recently reviewed.[48]

The estimation of f_{at} in outdoor environments presents a different challenge. While these outdoor environments do not have confining boundaries and localized inflow/outflow regions that dominate the flow patterns, effects due to atmospheric turbulence,[49,50] local wind and weather conditions, convection effects due to thermal gradients, and other environmental factors have to be taken into account. Furthermore, even in outdoor settings, the presence of high human density (such as at sporting events, social gatherings, and so on) could introduce significant anthropogenic effects on the dispersion and transport of respiratory aerosols.

As the aerosol plume from the host travels downstream, it spreads due to diffusion, entrainment, and turbulence-induced mixing. This results in a direction-dependent drop in concentration (aerosol particles per unit volume) with distance from the host. To further understand how this enters the estimation of the variable f_{at}, we introduce the variable V_s, which is the volume of air surrounding the face of the susceptible that would be inhaled by the susceptible (see Fig. 3). If the aerosol concentration near the host is
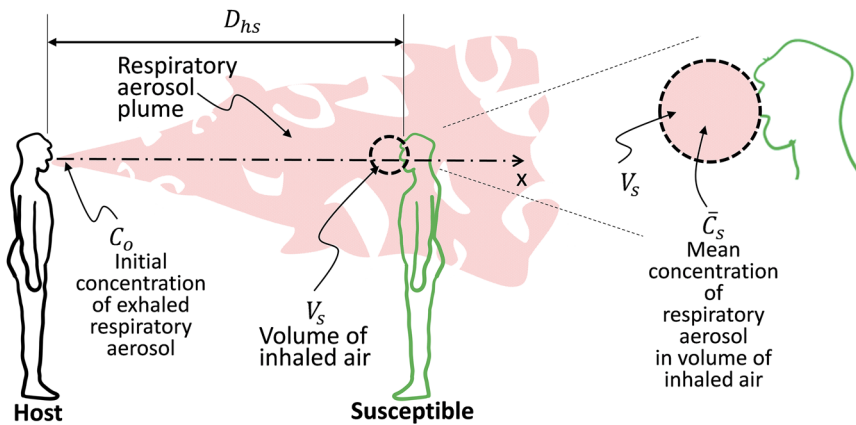
FIG. 3. Schematic depicting the inhalation volume of the susceptible that can be combined with the local concentration of the respiratory aerosol to estimate f_{at}.

C_o and the mean concentration in the volume V_s at a distance of D_{hs} is $\bar{C}_s$, then f_{at} due to this dilution in concentration can be expressed as $\bar{C}_s/C_o$. The volume V_s can be estimated given the inspiratory status of the susceptible (see the discussion of f_{is}), but in the current model, a choice for V_s that eliminates dependence of this variable on the susceptible is the maximum possible volume of air that can be inhaled by an adult per second, which is about 2 liters.[33] Thus, f_{at} can be estimated under these assumptions if $\bar{C}_s/C_o$ is known or can be estimated. We point out that the "exposure index" of Liu *et al.*[51] is defined in a similar way and, in their study, is estimated using computational modeling. It is also noted that C_o could be expressed in terms of the ratio of the particle expulsion rate to the exhalation rate of the host as $C_o = \dot{R}_h/\dot{V}_h$.

A number of studies have measured the spreading rate of the exhalation jets formed from various expiratory activities,[52–54] and this spreading rate can vary significantly with downstream distance for breathing, talking, and coughing. External flow currents and thermal convection[33] effects will however deform the shape of the expiratory plume and may enhance non-uniformity in the concentration of the respiratory aerosols within the jet. Quantifying the effect of all these factors is the key challenge in estimating f_{at}. In Sec. VIII, we will employ canonical computational models of scalar dispersion to provide estimates of the protection factor (PF) associated with physical distancing in several scenarios.

f_{vv} represents the fraction of respiratory aerosol particles from the infected host that arrive in the immediate vicinity of the susceptible with viable virions. Ambient air currents determine the "time-of-flight" of the aerosol particles, and this combines with temperature, humidity, and UV exposure to determine the viability of the virions carried in the aerosols. A study has shown that the SARS-CoV-2 virion can stay viable in an aerosol form for three or more hours,[13] but high temperature[55] and sunlight/UV exposure[56,57] are both detrimental to virion viability. Humidity, on the other hand, has a more complex effect on the viability of airborne viruses. For instance, three regimes of Influenza A virus viability in droplets, defined by relative humidity (RH), have been postulated: high viability at physiological (~100% RH) and dry (<50% RH) conditions and lower viability when intermediate humidity (50%–100% RH) exists in combination with high concentrations of naturally occurring biochemical solutes in the droplet.[58] This complex dependency

on humidity is likely the one factor that has made it difficult to correlate the transmission risk with regional and seasonal variations in environmental conditions.[59] In general, f_{vv} can be modeled as $e^{-T/\tau}$, where T is the time-of-flight and τ is the half-life of virions in an aerosolized form, which depends on the virus as well as the temperature, humidity, and UV exposure. A number of recent studies have measured τ for SARS-CoV-2 in a variety of settings.[13,56]

V. SUSCEPTIBLE RELATED VARIABLES

f_{is} is the fraction of bioaerosols from the host in the vicinity of the susceptible that would be inhaled and deposited in the respiratory tract of a susceptible not wearing a face covering. This variable primarily depends on the inspiratory status of the susceptible. At rest, an adult human inhales about 100 ml of air per second,[60] but this value can go up to 20-fold during intense exercise.[33] Within the context of the current model, f_{is} could be estimated as the ratio of the susceptible's inspiratory rate to the maximum possible inspiratory rate for a human (we denote this maximum ventilation rate as $\dot{V}_{max}$), which can be assumed to be 2000 ml/s.[33] We note that the volume here is the same as V_s in Sec. IV. With this prescription, f_{is} for the average healthy adult male could vary from 0.05 during rest to 1.0 during intense exercise. Beyond the exercise state of the individual, the tidal volume (volume inhaled per breath) and ventilation rate also depend on age,[61] gender, body weight,[62,63] and the respiratory health of the person, and these factors can be easily accounted for in f_{is}. For instance, the measured values of ventilation rates for women are about 20% lower than for men,[62] and this would translate to a 20% reduction in f_{is} for women. Similarly, short adults can have resting inspiratory rates that are about 20% lower than tall adults,[62] and this would result in a proportionate reduction in f_{is}. Inspiration rates for preteens can be threefold lower than adults,[61] and this would also reduce f_{is} proportionately. Thus, differential inspiration rates could play a role in the age and body-weight associated COVID-19 prevalence disparities noted in recent studies.[64,65] The effect of physical activity-associated changes in ventilation rates on the transmission risk is examined in Sec. VIII.

N_{ID} is the infectious dose for airborne transmission. In the arena of infectious diseases, the infectious dose is often expressed

as HID_{50},[22] which is the minimum infectious dose required to initiate infection in 50% of inoculated humans. This number is usually obtained via controlled studies where human volunteers are exposed to different viral loads. However, such studies are not available for potentially lethal viruses such as SARS-CoV-2. Studies on the infectious dose for Influenza A indicate a HID_{50} of O(1000) virus particles.[22,66] Studies of MERS-CoV in mice found a similar infectious dose,[67] so the HID_{50} for humans accounting for the larger body weight could be two or more orders of magnitude higher. It is important to note that for Influenza A, the infectivity via aerosols has been found to be $O(10^5)$ higher than via a nasopharyngeal (i.e., nasal swab) route,[68] highlighting the exceptional effectiveness of the airborne route for transmission of respiratory infections. The infectivity of airborne viruses also depends on the carrier droplet size. Small (~2 μm) droplets deposit deeper in the lungs and have been shown to be two or more orders of magnitude more infective than larger (>10 μm) droplets.[69] Finally, the infectious dose might also depend on the age and health status (including the level of immunity to infection) of the susceptible. The determination of N_{ID} for SARS-CoV-2 remains one of the most important tasks for scientists working in this arena.

The remaining variable T_s is the duration of exposure of the susceptible to the aerosols from the host. Based on the CAT inequality, if all other conditions remain stationary, the total number of viable virions transmitted is directly proportional to the exposure duration. The transmission is successful when this viral dose equals or exceeds the infectious dose (i.e., when $T_s \geq T_{sC}$).

VI. FACE COVERINGS

Face coverings appear in the two factors f_{mh} and f_{ms} as fractions of aerosols/droplets that pass through the face coverings of the host and susceptible, respectively, and there are much data available to estimate these variables. These face covering-related variables depend on two factors—the material of the face covering and the fit of the face covering on the face of the individual. A perfectly fit N95 face mask, for instance, stops 95% or more of the particles that go through it, and f_m would therefore be equal to 0.05 for such a mask. Thus, the wearing of a well-fit N95 mask by either the host or the susceptible could reduce the transmission risk by a factor of 20. Furthermore, if both individuals are wearing such masks, the transmission risk, according to the CTA inequality, could reduce by a factor of 400.

Surgical masks have been measured to block 30%–60% of respiratory aerosols,[70,71] and in another study, a surgical mask reduced aerosol shedding of Influenza A virions from infected hosts by a factor of 3.4.[28] This suggests that even surgical masks worn by both the host and the susceptible could reduce the transmission risk by factors ranging from about 2 to 10. Another recent study of viral shedding with and without surgical face masks from patients with Influenza, coronavirus (SARS), and rhinovirus provides clear evidence of the ability of such face coverings to reduce the transmissibility of the virus.[72] Finally, we point out that even home-made cloth masks provide some protection against airborne infections,[71] and in Sec. VIII, we will examine this in more detail for a range of fabrics.

The fitment of the mask is important for overall protection since a loose-fitting mask with perimeter leaks allows unfiltered aerosols to bypass the mask.[73] Leaks are a particular problem for outward protection (i.e., reducing emission of respiratory aerosols by the infected host) since the process of expiration pushes the mask outwards and enhances perimeter leaks.[11,74,75]

Finally, in addition to filtering aerosol particles, face coverings also reduce the velocity of exhalation jet.[74,76] This could increase the expansion angle of respiratory jet and reduce the initial penetration distance of the respiratory droplets,[77] thereby altering f_{at}. For instance, a recent study found that the fabric in some face coverings might facilitate the breakup of large droplets into smaller ones[78] and, in doing so, increase f_{at}, thereby increasing the transmission risk.

VII. MODEL PREDICTIONS

The model is now applied to address three distinct questions: what protection is afforded by different face coverings, how does the risk decrease with increased physical distance between the host and susceptible, and finally, to what degree does the level of physical activity, as manifested in the ventilation rates of the host and/or the susceptible, affect the transmission risk.

A. Protection afforded by face coverings

We start with the effect of face masks and employ data from the work of Zangmeister *et al.*[71] on the filtration efficiency (*FE*) of common fabrics used in respiratory face masks. These authors examined more than 30 different fabrics and quantified the filtration efficiency for droplet sizes ranging from particle mobility diameters (PMD) between 50 nm and 825 nm. Given that aerosol transmission may involve droplet sizes ranging up to 5 μm, we have estimated the lower and upper bounds of the average filtration efficiency ($\overline{FE}$) for particle sizes ranging from 50 nm to 5 μm (see the procedure in Appendix A). The fraction of aerosols/droplets that pass through the face coverings is then given by $f_m = 1 - \overline{FE}/100$. Given these values and the assumption that the filtration efficiency is the same for inward as well as outward protection (i.e., $f_{mh} = f_{ms} = f_m$), we can now estimate the unilateral protection factor (*PF*) if either the host or the susceptible wears this mask, as $PF = f_m^{-1}$. The corresponding bilateral protection factor, i.e., when both individuals wear masks, is then given by $PF = f_m^{-2}$. These PFs normalized by the corresponding situation where neither individual is wearing a mask are plotted in Fig. 4 for selected cases from the work of Zangmeister *et al.*[71]

Given the large uncertainties in estimates of the protection factor derived here, only general conclusions regarding the face masks are drawn here. First, a number of simple fabrics (Cotton 4, Cotton 14, and Synthetic Blend 2) provide protection factors that are similar or better than the Surgical Mask sample. Second, even the lower bound of unilateral protection for many of these samples exceeds 2.0, which represents a significant reduction in the transmission risk. Third, for bilateral protection, Cotton 4 and Synthetic Blend 2 have minimum protection factors that exceed 5. Finally, the true protection factors for these fabrics are likely significantly higher than the lower bounds established here. Indeed, if we average the upper and lower bounds of $\overline{FE}$ for the four most effective fabrics/samples
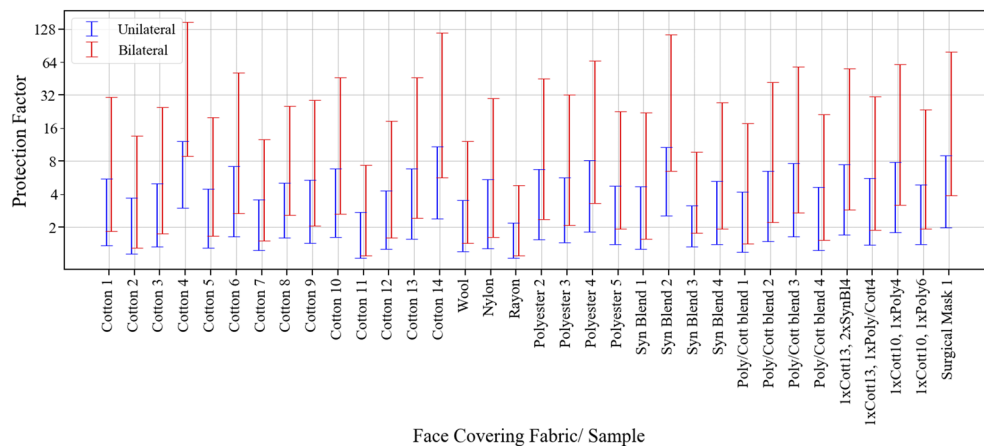
FIG. 4. Estimation of protection from aerosol transmission afforded by the donning of face coverings based on the published filtration efficiency data of Zangmeister *et al.*[71] for 34 different fabrics/samples. The protection factor (PF) is a quantity that is normalized by the risk of transmission associated with the situation when neither the host nor the susceptible wears a mask.

(Cotton 4, Cotton 14, Synthetic Blend 2, and Surgical Mask), we obtain an aggregate filtration efficiency of 63%, which would correspond to a unilateral (bilateral) protection factor of 2.7(7.3). Thus, simple face masks made from any of these fabrics/materials could significantly lower overall transmission rates. This effectiveness of face masks is being corroborated by recent epidemiological[16] and animal[79] studies of COVID-19 transmission. We point out that the above analysis ignores perimeter leaks, which can significantly deteriorate the effectiveness of face masks.[11] The analysis also does not account for unsteady and velocity dependent effects of expiratory events on the filtration efficiency.[74]

B. Protection due to physical distancing

The model is used next to examine the protection from transmission afforded by the physical distance between the host and the susceptible in an outdoor environment. As mentioned earlier, the distance between the host and the susceptible is a dominant factor in the variable f_{at} associated with the transport of virion-bearing aerosols. However, the estimates for the rate at which the transmission risk diminishes with distance between the host and the susceptible are not readily available. Here, we employ simple models of the aerosol dispersion to estimate the protection factor associated with physical distancing.

We start by assuming that the mean concentration in the inhaled volume of the susceptible is equal to $C(D_{hs})$, where C is the concentration at a height of 1.5 m above ground at any given distance from the host (see Fig. 5). Dispersion-induced dilution at a distance of D_{hs} would then result in $f_{at} \sim C(D_{hs})/C_o$, and a corresponding protection factor due to physical distancing of f_{at}^{-1}. Several scenarios for outdoor transmission are considered based on various combinations of expiration velocity (V_j), ambient wind speed (U_∞), and buoyancy induced effects. We note that these models are consistent with the approach inherent to the CAT inequality that assumes a sequential segregation of the various effects involved in airborne

transmission. In particular, important near-field effects such as droplet breakup and evaporation are assumed to be accounted for in the variable f_{ah} and are therefore not included in the droplet dispersion models discussed in the current section. The cases are as follows:

1. V_j and U_∞ are both of very low magnitude; this could correspond to a sedentary individual breathing at a low exhalation rate in still wind conditions. This situation can be modeled as normal diffusion dominated dispersion, and the analytical solution for steady-state diffusion from a point source[80] in an unbounded domain indicates that $C(x) \sim x^{-1}$, where x is the distance from the point source. The molecular diffusion will not be relevant since it will take a long time to establish itself (on the order of $t \sim x^2/\gamma$, where γ is the molecular mass diffusion coefficient, typically many hours in air). However, even relatively weak background turbulence with eddies smaller than x will generate turbulent diffusion coefficients[81] $\gamma_T \gg \gamma$ and also establish a $C(x) \sim x^{-1}$ spatial decay.

2. V_j significantly exceeds U_∞; this could correspond, for instance, to a person talking or singing (where expiratory flow speeds range up to 5 m/s[54]) in still wind conditions. This situation could be approximated as a turbulent jet in quiescent flows, and studies[82] of such flows in canonical configurations indicate that the peak concentration decays beyond the near field as $C(x) \sim x^{-1}$ in the direction of the jet. This situation has been analyzed recently for speech-driven aerosol transport including time dependence.[83]

3. U_∞ significantly exceeds V_j; this could correspond, for instance, to a person breathing normally with an expiratory velocity of ~ 1 m/s[84] on a windy day with wind velocities upwards of 10 miles/h. Neglecting buoyancy effects, this situation can be modeled as a horizontal plume from a point source in a crossflow, and studies[85,86] suggest that $C(x) \sim x^{-3/2}$ beyond the near-field region.
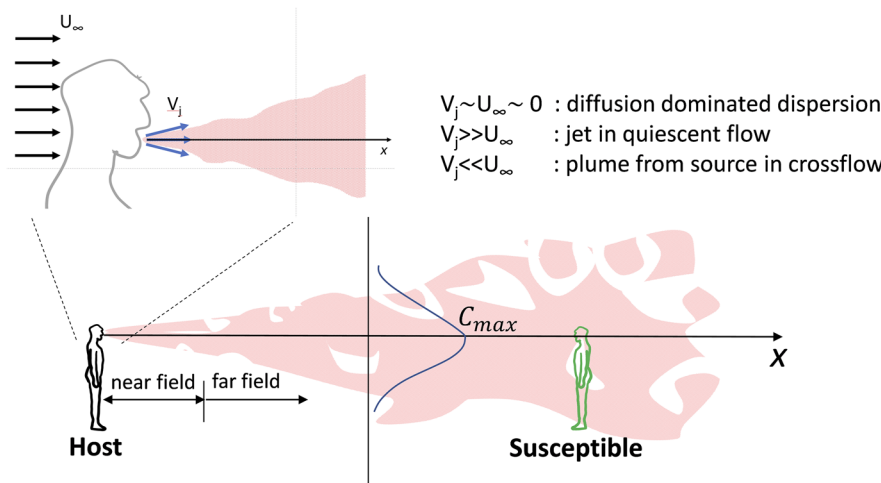
FIG. 5. Schematic showing various scenarios for which the effect of physical distancing on the transmission risk is assessed. The aerosol plume from the host consists of a near field, which can be highly variable, and a far field, where the plume exhibits more self-similar or universal characteristics within various classes of flow. The analysis in this section focuses on the far-field domain.

4. The previous situation of a horizontal plume does not account for buoyancy effects, and the data employed do not account for the time-dependent pulsatile nature of breathing. These effects can be included in the current model if data from appropriate computations or experiments are available. Here, we employ data generated from a wall-modeled large-eddy simulation[87] of a plume from a point source located 1.5 m above the ground in a turbulent atmospheric boundary layer, with a mean wind velocity corresponding to 2 m/s.[83] The model is designed to mimic normal breathing with the scalar (representing the respiratory aerosol) being released as puffs at regular intervals of 3 s. The exhaled breath is assumed to be at a temperature

of 37 $^{\circ}$C, and two ambient temperature conditions are considered: 0 $^{\circ}$C and 42 $^{\circ}$C. In the model, buoyancy effects are included using the Boussinesq approximation. The incoming wind flow itself is assumed to be unstratified and neutrally buoyant. The reader is referred to Appendix B for details about the methodology of the simulations.

Figure 6(a) shows a plot of the instantaneous scalar concentration for the second case, and Figs. 6(b) and 6(c) show the time-averaged plume concentrations for both cases. As expected, the plume rises for the first case (the "light" plume) but descends toward the ground for the second case ("heavy" plume) due to buoyancy
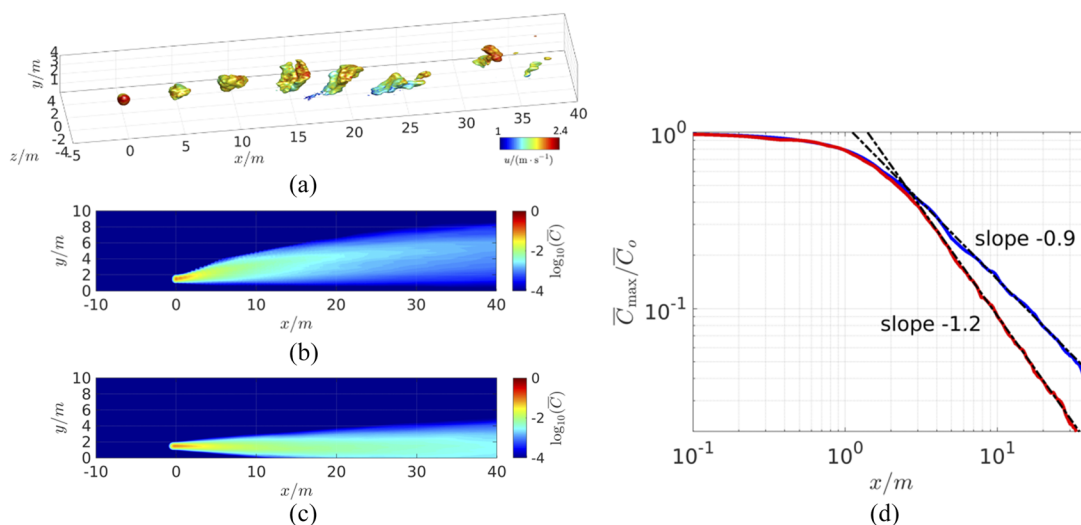
FIG. 6. Results from the wall-modeled large eddy simulation (LES) of a breath generated aerosol plume (at $x = 0$) in a turbulent boundary layer. (a) Isosurfaces of instantaneous concentration of scalar $C/C_o = 0.01$, colored by the local streamwise velocity showing the breath aerosol puffs being transported in the turbulent flow, (b) contours of the mean concentration for a plume that is warmer than the ambient flow, and (c) contours of the mean concentration for a plume that is colder than the ambient flow. (d) Mean concentration with the streamwise distance (in meters) at a height of 1.5 m from the ground along with best fit power laws beyond the near-field region.
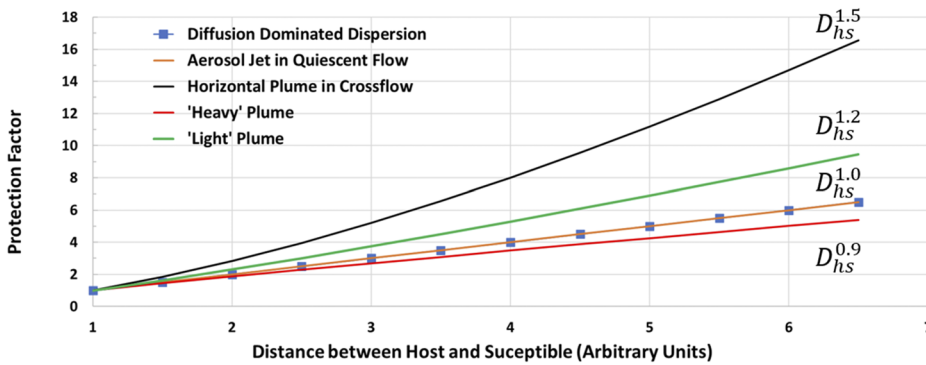
FIG. 7. Estimate of the protection factor as a function of physical distance (in arbitrary units) between the host and susceptible for the five scenarios examined here. The protection factor is normalized for each case by the condition where both the host and susceptible are at a unit distance. The protection factor is inversely proportional to the decay of the concentration with distance between the host and the susceptible D_{hs}.

effects for the very hot surrounding air case into which the cooler and denser air is exhaled. Figure 6(d) shows the maximum concentration of the respiratory plumes as a function of distance for the two cases, and we find that beyond a distance of about 3 m, the plume concentration decays consistently as $C(x) \sim (x^{-1.2})$ and $C(x) \sim x^{-0.9}$ for the light and heavy plumes, respectively. Thus, the presence of the ground as well as buoyancy has a noticeable effect on the concentration decay rate.

Figure 7 shows the protection factors due to physical distancing for all the cases discussed above, and we note that since the y-intercepts of all the curves have been individually normalized to unity at a unit distance, a direct numerical comparison between the two conditions is not appropriate. The plot does however indicate that in the absence of a crossflow, the protection factor increases linearly with distance, whereas when the crossflow velocity is significantly larger than the exhaled jet velocity, the protection factor increases at a faster rate of $D_{hs}^{1.5}$. Furthermore, the buoyancy has a noticeable effect on the decay of aerosol concentration, and the downward movement of a heavy plume combined with the confinement due to the ground could potentially diminish the protection afforded by physical distancing. Given that wind conditions can be highly variable, a conservative estimate from the above analysis is that physical distancing affords approximately a linear

increase in protection from transmission. The analysis also demonstrates the use of data from computational fluid dynamics models to parameterize the model for specific scenarios.

C. Level of physical activity and transmission risk

The final application of the model is to examine the potential effect of physical/exercise intensity on the risk of transmission. This would be relevant to settings, such as gyms, sports/exercise facilities, and even gatherings/events, schools, and workplace situations where levels of physical activity might exceed levels that are considered sedentary. The exercise intensity enters the CAT inequality through the ventilation rates of the host and the susceptible. As pointed out earlier, in expiratory activities such as breathing and talking, the particle expulsion rate may be estimated as $\dot{R}_h = n_{dh}\dot{V}_{Eh}$, where n_{dh} is the number of droplets emitted per volume of exhaled gas (and may be assumed to be constant for a given host) and $\dot{V}_{Eh}$ is the ventilation rate of the host. The variable f_{is} is equal to the rate of the susceptible's ventilation rate divided by the maximum possible ventilation rate, i.e., $f_{is} = \dot{V}_{Es}/\dot{V}_{max}$. Employing established definitions[88] that relate exercise intensity to oxygen consumption rates, and further assuming proportionality between oxygen consumption rates and corresponding ventilation rates, and that the maximum ventilation
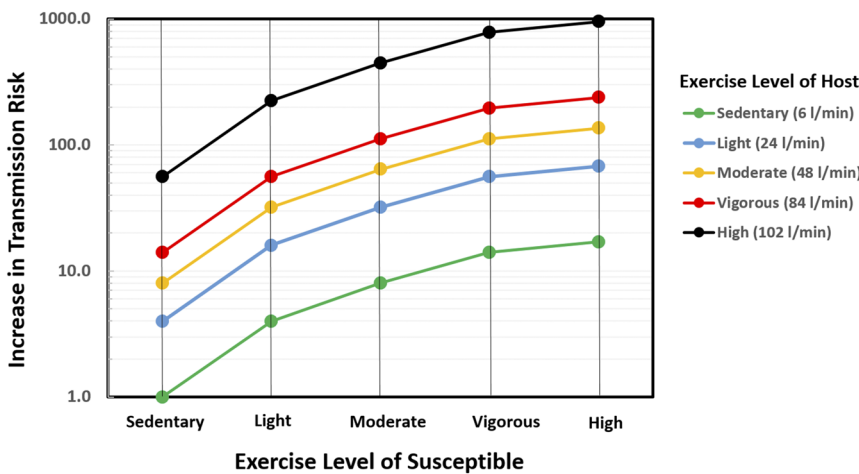

FIG. 8. Estimate of the transmission risk increase due to physical activity/exercise induced increased ventilation rates for hosts and susceptibles. The assumed ventilation rate for each of the five levels is included in the legend. The increase in the transmission risk is normalized by the condition where both the host and susceptible are sedentary (sleeping or sitting).

rate $\dot{V}_{max}$ for adults is 2 l/s,[89] we can estimate the increased transmission risk with exercise intensity over the sedentary condition as $\left(\dot{R}_h f_{is}\right)/\left(\dot{R}_{h,min} f_{is,min}\right) = \dot{V}_{Eh} \times \dot{V}_{Es}/\dot{V}_{min}^2$, where $()_{min}$ corresponds to an adult in a sedentary condition. In the current estimation procedure, $\dot{V}_{min}$ is set at 100 ml/s, which is 5% of the maximum ventilation rate, and the ventilation rates for the intermediate levels are based on the measured values for adults.[88]

Figure 8 shows this increased transmission risk for the five exercise intensity levels, and it can be seen that even for a susceptible in a sedentary state, the transmission risk goes up by a factor of eight if the host is at a moderate intensity of exercise. In settings such as shopping malls, outdoor markets, warehouses, or high-schools, where activity levels of hosts and susceptibles could be in the light to moderate range, the increase in the transmission risk just due to increased ventilation rates would, according to the current model, be up to 64 times higher. In a facility such as a gym or, for instance, a basketball practice, where exercise intensity levels could be in the "vigorous" range, the transmission risk could be nearly 200 times higher due to increased exhalation and inhalation rates of the individuals involved. A survey of the existing literature indicates that this increase in risk with a physical activity level associated with various common scenarios is under-appreciated.

VIII. COMPARISON WITH OTHER INFECTION RISK MODELS

Existing models for estimating the infection risk via airborne transmission can be classified into the Wells–Riley type and dose–response models.[90] Within this context, the current model should be considered a dose–response model since it explicitly makes use of the infectious dose (N_{ID}) to predict the infection risk. The current model, as proposed, can further be characterized as a deterministic (as opposed to stochastic) dose–response model since it assumes that a dose larger than the threshold dose of N_{ID} results in an infection.[90]

The Wells–Riley type models are based on the notion of an infectious "quantum" that is defined as the quantity of expelled aerosols required to cause an infection in a susceptible.[21,24] Within the context of the CAT inequality, the quantum emission rate can be expressed as $\left(\dot{R}_h f_{vh}/N_{ID}\right)$, and the CAT inequality could easily be reformulated to express risk in terms of this quantity. However, the quantum emission rate combines a host-dependent variable (the rate of viral shedding) with a susceptible dependent variable (the infectious dose) and makes it difficult to delineate the effects of the distinct states (health, inspiratory state, mask use, and so on) of the two individuals involved. Furthermore, the vast majority of such models assume a "well-mixed" state for the aerosols in the environments, and this does not allow for "local" effects[90] that have direct bearing on practices such as social distancing.

The dose–response models of varying degree of complexity have been developed.[90] Many of these models allow for spatial and temporal inhomogeneities in the aerosol concentrations and are well suited for detailed modeling of infection risk in a variety of scenarios. Some of the recent models that have been developed can incorporate data on ambient flow conditions from computational models or experimental measurements.[91] However, such models are expressed in mathematically complex forms, which diminish

comprehensibility outside disciplinary expertise, and make it particularly difficult to communicate the underlying ideas to non-scientists. As shown in Secs. VII A–VII C, the simple mathematical form of the current model and its phenomenology-based compartmentalization into host, environment, and susceptible dependent variables not only allow for easier comprehension by a wide range of audiences but also provide quick estimates of factors including, but not limited to, the type of mask worn, physical distancing, and inspiratory status of the host and susceptible.

Finally, we point out the left-hand side of the CAT inequality represents the total aerosol viral dose inhaled by the susceptible, and if we denote this variable by $N_{Ds} = \dot{R}_{tot} T_s$, then $\left(\frac{N_{Ds}}{N_{ID}} - 1\right)$ represents the normalized viral "overdose" delivered to the susceptible. Thus, in addition to evaluating the risk of transmission, the CAT inequality can also be used to assess the degree of exposure of the susceptible to aerosolized viruses, which is known to be correlated with the severity of the infection.[92]

IX. CAVEATS

The notion that "a model is a lie that helps us to see the truth"[103] certainly applies to the current model as well. The CAT inequality is an attempt to express the highly complex, multifactorial process of airborne transmission of a respiratory infection such as COVID-19 in a simple way, and the following caveats and limitations of this model are worth pointing out:

1. The choice of the variables in the CAT inequality is not unique, and other combinations of the variables are possible. In particular, the variables shown in the CAT inequality could be decomposed further; for instance, $\dot{R}_h$ can be expressed as the rate of droplet generation in the respiratory tract and the fraction of generated droplets that are expelled from the mouth. Such a variable separation might be appropriate, for instance, to isolate the effect of therapies that attempt to diminish the droplet generation rate via alteration of the mucous properties.[35]

2. The inequality assumes that the rate of arrival of virion-bearing aerosols in the vicinity of the susceptible is constant in time. The recent analysis[83] of speech driven aerosol transport takes into account the start time and travel duration in scenario (2) treated in Sec. VIII. The CAT inequality could be modified to include a time-dependent emission and arrival rate,[21] but this would increase the complexity of the mathematical expression. Assuming the steady state condition results in predictions that are more conservative in most cases. Finally, it is also assumed here that the rate of virion arrival (i.e., proportional to the advective or diffusive flux of C) in the vicinity of the susceptible is sufficiently high so that the local concentration is not markedly affected by the inhalation process itself. If the flux is not high enough, the inhalation may deplete the concentration near the susceptible over time. The analysis for flux-limited situations again introduces additional complexities.

3. The CAT inequality could be missing important but as yet unknown effects. For instance, the use of N_{ID} in the model assumes that it is the accumulated dose of virus that determines transmission. While this assumption is quite standard

in the arena of infectious diseases,[21–23] it is plausible that the rate at which this infectious dose is delivered to the respiratory tract of the susceptible is also important in initiating an infection. For instance, 1000 virions inhaled over a short duration (say minutes) might overwhelm the immune system, whereas the same viral dose delivered over a much longer duration (say hours) might allow the immune system to mount an effective response and avoid infection.

4. The variables in the CAT inequality are more accurately represented as variables with probability density functions (PDFs) given the stochastic nature of the processes involved.[93] For instance, respiratory droplets of different sizes are expelled at different rates[9,28,31,36] during an expiratory event, and the rate of droplet emission $\dot{R}_h$ could therefore be expressed as a droplet size-dependent PDF. Similarly, the viral loading of respiratory droplets (f_{vh}) as well as the infectious dose N_{ID} are expected to be functions of droplet size and could therefore be represented by droplet size dependent PDFs. The environment determining f_{at} is most often highly turbulent and is expected to cause significant fluctuations in travel time, turbulent diffusion rates and individual eddying events can influence the local concentrations. Hence, the factor f_{at} itself has a mean value as well as a distribution around that mean value that depends on detailed flow conditions.

5. If the variables in the CAT inequality are interpreted as random variables with PDFs (as in the previous point), it implicitly assumes the variables and factors are statistically independent. However, variables in the CAT inequality are not necessarily mutually independent given the fact that many of them have common dependencies. The joint dependency of many variables on particle size has already been described above. Other examples include the face covering on the host, which modifies f_{mh}. A resulting alteration of the expiratory jet due to the mask could also affect the aerosolization variable f_{ah} of the expelled droplets as well as entrainment into the ambient air current, which could affect f_{at}.

6. The model assumes a single host, but the CAT inequality can easily account for multiple hosts by summing the left-hand side for multiple infected hosts.

7. The validation of the proposed model is not attempted here. The validation requires accurate estimates of inputs as well as outputs to the models, and these are difficult to obtain, especially for potentially lethal infections such as COVID-19. Indeed, most models of airborne infection to date, including classic[24] as well as more recent models,[21,94–96] remain unvalidated. Despite this lacuna of validation, the value of all such models, including the current one, is that they enable an examination of how transmission risk scales with key variables and an assessment of the effects of mitigation strategies on overall transmission rates.

X. SUMMARY

The CAT inequality is a mathematical model for estimating the risk of airborne transmission of infectious diseases such as COVID-19, which is expressed in a simple and intuitive way so as to convey the factors involved in transmission to a wide range of stakeholders ranging from scientists from various disciplines to policy makers, public media, and even the general public. As shown through specific examples, the model provides a framework for interpreting and quantifying the relative changes in risk from behaviors such as, but not limited to, wearing masks, physical distancing, and the intensity of physical activity/exercise on infection risk, in terms that are easy to convey to a range of audiences. The approximately inverse relationship of the transmission risk and spatial distance from physical distancing is one example of the important insights that can be generated by the model.

In closing, we point out that while the transmission model presented here is inspired by the Drake equation, we understand much more about the factors involved in this transmission model than we do about the factors in the Drake equation. Indeed, as discussed in the paper, estimates for many of the variables in the CAT inequality can be obtained from existing data or from basic principles of fluid dynamics, physiology, and virology. Even for the variables for which we currently do not have good estimates, we understand the underlying dependencies as well as the procedures/methods required to estimate these variables, and it is expected that ongoing studies will close these gaps in our understanding and provide better quantification of all the variables involved in this model.

APPENDIX A: ESTIMATION OF UPPER AND LOWER BOUNDS FOR AVERAGE FILTRATION EFFICIENCY OF FACE MASK FABRICS

The procedure for estimating the lower and upper bounds of the filtration efficiency (FE) for various fabrics in Fig. 4 is described here. Zangmeister et al.[71] measured the FE for various fabrics as a function of particle mobility diameters (PMDs) that range from 50 nm to 825 nm. However, it is well established that aerosol transmission occurs with aerosol particles with diameters up to at least 5 μm. In order to apply the data from the work of Zangmeister et al.[71] in a way that is relevant for airborne transmission, the FE vs PMD data have to be extended up to 5 μm. However, the FE dependence on PMD is affected by the filter diameter, the solidity (1-porosity), the density of the particles, and the face velocity, and simple extrapolations of the FE vs PMD curves are not possible. Given this, and the fact that FE for any given material approaches 100% at high enough PMD, we derive a lower and upper bound of the average FE over the 50 nm–5000 nm range as follows (see Fig. 9): the lower bound is obtained by assuming that the FE for PMDs greater than 825 nm is
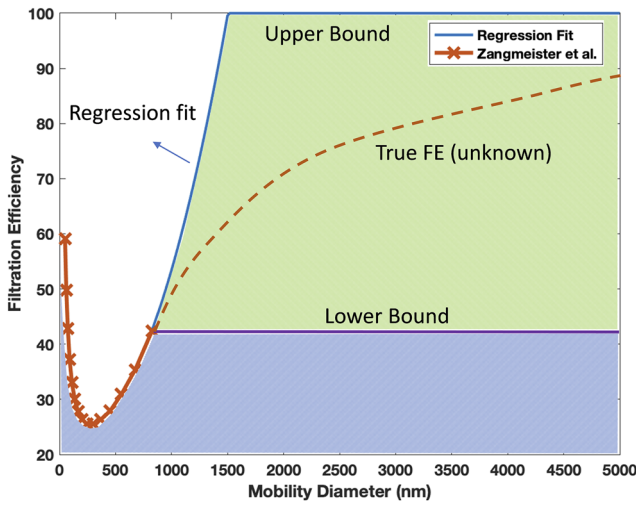
FIG. 9. Depiction of methodology for estimating the lower and upper bound of the average FE over the 50 nm–5000 nm range from the data of Zangmeister et al.[71] This particular example is for the 1× Cotton 13, 2× Synthetic Blend 4 sample. The lower bound is obtained by assuming that the FE for PMDs greater than 825 nm is equal to the FE measured at 825 nm. The upper bound is obtained by employing a regression fit to the right side of the measured curve (beyond the PMD for minimum FE) and extending it to the FE = 100% line. Beyond this, the FE for the upper bound is assumed to equal 100%.

equal to the measured FE at 825 nm. The upper bound is obtained by employing a regression fit to the right side of the measured curve (beyond the PMD for minimum FE) and extending it to FE = 100%. Beyond this, the FE for the upper bound is assumed to be equal to 100%. A quadratic regression fit results in an R^2 value exceeding 0.90 for all cases. For each bound, the average FE (denoted by $\overline{FE}$) over the PMD range 50 nm–5000 nm can now be estimated using numerical integration. Figure 9 illustrates the areas used in the calculation of these bounds for one case, and Table I shows the $\overline{FE}$ computed in this way for the various fabrics considered in the current study. Finally, Table I provides a brief description of the various fabrics/samples from the work of Zangmeister et al.[71] that are included in the current study, along with the estimated lower and upper bounds of the average filtering efficiencies.

APPENDIX B: WALL-MODELED LARGE EDDY SIMULATION OF BREATH AEROSOLS IN TURBULENT FLOWS

The transport of periodically released breath puffs in a turbulent atmospheric boundary layer is simulated by wall-modeled large eddy simulation (LES). The computational domain is 60 m, 10 m, and 20 m in the streamwise (x), wall-normal (y), and spanwise (z) directions, respectively, with $672 \times 117 \times 384$ grid points. The point source corresponding to the host is placed 1.5 m above from the ground, 10 m downstream of the inflow (defined as x = 0), and at the middle span. The Reynolds number based on the bulk velocity (2 m/s), the emission height (1.5 m), and the viscosity of air is 2.0×10^5. The grid has a uniform spac-

TABLE I. Description of the various fabrics/samples from the work of Zangmeister et al.[71] that are included in the current study.

No.	Axis legend	Name in paper (ID, structure, yarns/in.)	$\overline{FE}$ lower bound	$\overline{FE}$ upper bound
1	Cotton 1	Cotton 1, plain weave, 152	26.0	81.9
2	Cotton 2	Cotton 2, plain weave, 152	12.0	72.8
3	Cotton 3	Cotton 3, plain weave, 152	24.1	79.8
4	Cotton 4	Cotton 4, plain weave, 229	66.4	91.8
5	Cotton 5	Cotton 5, sateen, weave, 356	22.1	77.7
6	Cotton 6	Cotton 6, satin weave, 812	38.9	86.0
7	Cotton 7	Cotton 7, poplin weave, 89	18.5	71.8
8	Cotton 8	Cotton 8, block weave, 102	37.7	80.1
9	Cotton 9	Cotton 9, poplin weave, 152	30.1	81.3
10	Cotton 10	Cotton 10, poplin weave, 152	38.4	85.3
11	Cotton 11	Cotton 11, plain weave, 152	4.4	63.2
12	Cotton 12	Cotton 12, knit, 100	20.7	76.8
13	Cotton 13	Cotton 13, satin weave, 600	35.8	85.3
14	Cotton 14	Cotton 14, quilt batting	57.9	90.8
15	Wool	Wool, plain weave, 101	16.1	71.3
16	Nylon	Nylon, poplin weave, 127	21.4	81.6
17	Rayon	Rayon, plain weave, 152	4.6	54.3
18	Polyester 2	Polyester 2, plain weave, 152	34.6	85.1
19	Polyester 3	Polyester 3, poplin weave, 152	30.6	82.3
20	Polyester 4	Polyester 4, poplin weave, 152	45.0	87.7
21	Polyester 5	Polyester 5, poplin weave, 229	28.0	79.0
22	Syn blend 1	Syn blend 1, poplin weave, 330	20.0	78.7
23	Syn blend 2	Syn blend 2, twill weave, 203	60.7	90.6
24	Syn blend 3	Syn blend 3, waffle weave, 25	24.6	67.9
25	Syn blend 4	Syn blend 4, poplin weave, 229	27.7	80.9
26	Poly/cott blend 1	Poly/cott blend 1, plain weave, 229	15.6	76.1
27	Poly/cott blend 2	Poly/cott blend 2, poplin weave, 152	32.6	84.5
28	Poly/cott blend 3	Poly/cott blend 3, twill weave, 229	39.0	86.9
29	Poly/cott blend 4	Poly/cott blend 4, twill weave, 203	18.6	78.3
30	1× cotton 10, 1× polyester 4	1× cotton 10, 1× polyester 4	41.1	86.6
31	1× cotton 13, 2× syn blend 4	1× cotton 13, 2× syn blend 4	26.9	82.0
32	1× cotton 10, 1× polyester 6	1× cotton 10, 1× polyester 6	43.8	87.2
33	1× cotton 13, 1× poly/cotton 4	1× cotton 13, 1× poly/cotton 4	27.9	79.3
34	Surgical mask 1	Surgical mask 1, multi-layer	49.3	88.8

ing of 5 cm for y ≤ 3 m and −5 m ≤ x ≤ 10 m, as well as in the z direction. It is stretched in the (x–y) plane for y > 3 m, x < −5 m, and x > 10 m with a maximum stretching ratio of 4%.

The number of infectious respiratory aerosols and the temperature fluctuation around the ambient temperature are modeled as two transported scalar fields. The droplet evolution is represented using the Eulerian approach where instead of solving the Lagrangian evolution of individual drops, their concentration is treated as a passive scalar. This approach can be far less expensive numerically and is justified at the low volume fractions[34] and negligible terminal velocities associated with the small aerosolized droplets whose time-evolving concentration field the simulations aim to represent. See Refs. [97–99] for prior developments and applications of the fast Eulerian two-fluid approach. The release of the virus-laden puffs is implemented as a localized volume source term in the scalar transport equation. The buoyancy due to temperature variations is modeled in the momentum equation by the Boussinesq approximation as a function of the temperature. Subgrid-scale contributions for both the momentum are modeled by the Lagrangian-averaged dynamic eddy-viscosity model.[100,101] For the scalars, constant subgrid-scale Schmidt and Prandtl numbers Sc = Pr = 0.4 are used. Both the velocity and scalars are periodic in the spanwise direction. In the streamwise direction, the flow is periodic, while the scalars have a uniform Dirichlet boundary condition at the inflow and a convective condition at the outflow. A sponge layer is applied near the outflow to force the scalars to be zero and let the flow recover to a canonical turbulent boundary layer. For both the velocity and scalar, an equilibrium rough wall model with z_o = 0.5 mm is applied at the bottom wall and zero vertical gradient condition at the top boundary. The value of the scalar at the wall is the same as it is in the incoming air at the inflow. The equations of motion and scalar transport are solved using second-order accurate (in time and space) derivatives on a staggered mesh. The code is parallelized using MPI and has been widely validated in similar types of turbulent flows.[87,102] Statistics are collected over 30 min of physical flow time after the statistical steady state is reached. Increasing the number of grid points by 26% in each direction (i.e., doubling the total number of grid points) has a negligible effect on the flow statistics and the results presented in the main text.

DATA AVAILABILITY

The data that support the findings of this study are available from the corresponding author upon reasonable request.

REFERENCES

[1]L. Morawska and J. Cao, "Airborne transmission of SARS-CoV-2: The world should face the reality," Environ. Int. **139**, 105730 (2020).

[2]L. Morawska and D. K. Milton, "It is time to address airborne transmission of COVID-19," Clin. Infect. Dis. (published online 2020).

[3]D. Lewis, "Mounting evidence suggests coronavirus is airborne—But health advice has not caught up," Nature **583**(7817), 510–513 (2020).

[4]A. Mandavilli, 239 Experts With One Big Claim: The Coronavirus Is Airborne, The New York Times, July 4, 2020.

[5]WHO agrees with more than 200 medical experts that COVID-19 may spread via the air https://www.usatoday.com/in-depth/news/2020/04/03/coronavirus-protection-how-masks-might-stop-spread-through-coughs/5086553002/; accessed July 26, 2020.

[6]C. Y. H. Chao, M. P. Wan, L. Morawska, G. R. Johnson, Z. D. Ristovski, M. Hargreaves, K. Mengersen, S. Corbett, Y. Li, X. Xie, and D. Katoshevski, "Characterization of expiration air jets and droplet size distributions immediately at the mouth opening," J. Aerosol Sci. **40**(2), 122–133 (2009).

[7]S. Asadi, A. S. Wexler, C. D. Cappa, S. Barreda, N. M. Bouvier, and W. D. Ristenpart, "Aerosol emission and superemission during human speech increase with voice loudness," Sci. Rep. **9**(1), 2348 (2019).

[8]X. Xie, Y. Li, H. Sun, and L. Liu, "Exhaled droplets due to talking and coughing," J. R. Soc., Interface **6**(Suppl. 6), 6S703–S714 (2009).

[9]J. P. Duguid, "The size and the duration of air-carriage of respiratory droplets and droplet-nuclei," Epidemiol. Infect. **44**(6), 471–479 (1946).

[10]J. Wei and Y. Li, "Airborne spread of infectious agents in the indoor environment," Am. J. Infect. Control **44**(Suppl. 9), S102–S108 (2016).

[11]R. Mittal, R. Ni, and J.-H. Seo, "The flow physics of COVID-19," J. Fluid Mech. **894**, F2 (2020).

[12]E. Petersen, M. Koopmans, U. Go, D. H. Hamer, N. Petrosillo, F. Castelli, M. Storgaard, S. A. Khalili, and L. Simonsen, "Comparing SARS-CoV-2 with SARS-CoV and Influenza pandemics," Lancet Infect. Dis. **20**(9), e238–e244 (2020).

[13]N. van Doremalen, T. Bushmaker, D. H. Morris, M. G. Holbrook, A. Gamble, B. N. Williamson, A. Tamin, J. L. Harcourt, N. J. Thornburg, S. I. Gerber, J. O. Lloyd-Smith, E. de Wit, and V. J. Munster, "Aerosol and surface stability of SARS-CoV-2 as compared with SARS-CoV-1," N. Engl. J. Med. **382**, 1564 (2020).

[14]Coronavirus Disease (COVID-19) Situation Reports https://www.who.int/emergencies/diseases/novel-coronavirus-2019/situation-reports; accessed July 26, 2020.

[15]L. Morawska, J. W. Tang, W. Bahnfleth, P. M. Bluyssen, A. Boerstra, G. Buonanno, J. Cao, S. Dancer, A. Floto, F. Franchimon, C. Haworth, J. Hogeling, C. Isaxon, J. L. Jimenez, J. Kurnitski, Y. Li, M. Loomans, G. Marks, L. C. Marr, L. Mazzarella, A. K. Melikov, S. Miller, D. K. Milton, W. Nazaroff, P. V. Nielsen, C. Noakes, J. Peccia, X. Querol, C. Sekhar, O. Seppänen, S.-i. Tanabe, R. Tellier, K. W. Tham, P. Wargocki, A. Wierzbicka, and M. Yao, "How can airborne transmission of COVID-19 indoors be minimised?," Environ. Int. **142**, 105832 (2020).

[16]V. C.-C. Cheng, S.-C. Wong, V. W.-M. Chuang, S. Y.-C. So, J. H.-K. Chen, S. Sridhar, K. K.-W. To, J. F.-W. Chan, I. F.-N. Hung, P.-L. Ho, and K.-Y. Yuen, "The role of community-wide wearing of face mask for control of coronavirus disease 2019 (COVID-19) epidemic due to SARS-CoV-2," J. Infect. **81**(1), 107–114 (2020).

[17]S. E. Eikenberry, M. Mancuso, E. Iboi, T. Phan, K. Eikenberry, Y. Kuang, E. Kostelich, and A. B. Gumel, "To mask or not to mask: Modeling the potential for face mask use by the general public to curtail the COVID-19 pandemic," Infect. Dis. Model. **5**, 293–308 (2020).

[18]COVID-19 Map https://coronavirus.jhu.edu/map.html; accessed Aug 2, 2020.

[19]M. M. Ćirković, "The temporal aspect of the Drake equation and SETI," Astrobiology **4**(2), 225–231 (2004).

[20]M. J. Burchell, "W(h)ither the Drake equation?," Int. J. Astrobiol. **5**(3), 243–250 (2006).

[21]G. Buonanno, L. Stabile, and L. Morawska, "Estimation of airborne viral emission: Quanta emission rate of SARS-CoV-2 for infection risk assessment," Environ. Int. **141**, 105794 (2020).

[22]S. Yezli and J. A. Otter, "Minimum infective dose of the major human respiratory and enteric viruses transmitted through food and the environment," Food Environ. Virol. **3**(1), 1–30 (2011).

[23]L. Gammaitoni and M. C. Nucci, "Using a mathematical model to evaluate the efficacy of TB control measures," Emerging Infect. Dis. **3**(3), 335–342 (1997).

[24]E. C. Riley, G. Murphy, and R. L. Riley, "Airborne spread of measles in a suburban elementary school," Am. J. Epidemiol. **107**(5), 421–432 (1978).

[25]G. R. Johnson and L. Morawska, "The mechanism of breath aerosol formation," J. Aerosol Med. Pulm. Drug Delivery **22**(3), 229–237 (2009).

[26]J. Lee, D. Yoo, S. Ryu, S. Ham, K. Lee, M. Yeo, K. Min, and C. Yoon, "Quantity, size distribution, and characteristics of cough-generated aerosol produced by patients with an upper respiratory tract infection," Aerosol Air Qual. Res. **19**(4), 840–853 (2019).

[27]K. P. Fennelly, "Particle sizes of infectious aerosols: Implications for infection control," Lancet Respir. Med. **8**, 914 (2020).

[28]D. K. Milton, M. P. Fabian, B. J. Cowling, M. L. Grantham, and J. J. McDevitt, "Influenza virus aerosols in human exhaled breath: Particle size, culturability, and effect of surgical masks," PLoS Pathog. **9**(3), e1003205 (2013).

[29]W. G. Lindsley, T. A. Pearce, J. B. Hudnall, K. A. Davis, S. M. Davis, M. A. Fisher, R. Khakoo, J. E. Palmer, K. E. Clark, I. Celik, C. C. Coffey, F. M. Blachere, and D. H. Beezhold, "Quantity and size distribution of cough-generated aerosol particles produced by Influenza patients during and after illness," J. Occup. Environ. Hyg. **9**(7), 443–449 (2012).

[30]V. Stadnytskyi, C. E. Bax, A. Bax, and P. Anfinrud, "The airborne lifetime of small speech droplets and their potential importance in SARS-CoV-2 transmission," Proc. Natl. Acad. Sci. U. S. A. **117**(22), 11875–11877 (2020).

[31]Z. Y. Han, W. G. Weng, and Q. Y. Huang, "Characterizations of particle size distribution of the droplets exhaled by sneeze," J. R. Soc., Interface **10**(88), 20130560 (2013).

[32]Y. Bai, L. Yao, T. Wei, F. Tian, D.-Y. Jin, L. Chen, and M. Wang, "Presumed asymptomatic carrier transmission of COVID-19," JAMA **323**(14), 1406–1407 (2020).

[33]A. Nicolò, M. Girardi, I. Bazzucchi, F. Felici, and M. Sacchetti, "Respiratory frequency and tidal volume during exercise: Differential control and unbalanced interdependence," Physiol. Rep. **6**(21), e13908 (2018).

[34]L. Morawska, G. R. Johnson, Z. D. Ristovski, M. Hargreaves, K. Mengersen, S. Corbett, C. Y. H. Chao, Y. Li, and D. Katoshevski, "Size distribution and sites of origin of droplets expelled from the human respiratory tract during expiratory activities," J. Aerosol Sci. **40**(3), 256–269 (2009).

[35]D. A. Edwards, J. C. Man, P. Brand, J. P. Katstra, K. Sommerer, H. A. Stone, E. Nardell, and G. Scheuch, "Inhaling to mitigate exhaled bioaerosols," Proc. Natl. Acad. Sci. U. S. A. **101**(50), 17383–17388 (2004).

[36]G. R. Johnson, L. Morawska, Z. D. Ristovski, M. Hargreaves, K. Mengersen, C. Y. H. Chao, M. P. Wan, Y. Li, X. Xie, D. Katoshevski, and S. Corbett, "Modality of human expired aerosol size distributions," J. Aerosol Sci. **42**(12), 839–851 (2011).

[37]J. Fiegel, R. Clarke, and D. A. Edwards, "Airborne infectious disease and the suppression of pulmonary bioaerosols," Drug Discovery Today **11**(1–2), 51–57 (2006).

[38]X. Xie, Y. Li, A. T. Y. Chwang, P. L. Ho, and W. H. Seto, "How far droplets can move in indoor environments? Revisiting the wells evaporation? Falling curve," Indoor Air **17**(3), 211–225 (2007).

[39]D. Lohse, "Die abstandsregel in zeiten von corona," Phys. J. **19**(5), 18–19 (2020).

[40]J. Gralton, E. Tovey, M.-L. McLaws, and W. D. Rawlinson, "The role of particle size in aerosolised pathogen transmission: A review," J. Infect. **62**(1), 1–13 (2011).

[41]M. Small, C. K. Tse, and D. M. Walker, "Super-spreaders and the rate of transmission of the SARS virus," Physica D **215**(2), 146–158 (2006).

[42]W. F. Wells, "On air-borne infection*," Am. J. Epidemiol. **20**(3), 611–618 (1934).

[43]T. Dbouk and D. Drikakis, "On coughing and airborne droplet transmission to humans," Phys. Fluids **32**(5), 053310 (2020).

[44]P. J. Drivas, P. A. Valberg, B. L. Murphy, and R. Wilson, "Modeling indoor air exposure from short-term point source releases," Indoor Air **6**(4), 271–277 (1996).

[45]D. Licina, A. Melikov, J. Pantelic, C. Sekhar, and K. W. Tham, "Human convection flow in spaces with and without ventilation: Personal exposure to floor-released particles and cough-released droplets," Indoor Air **25**(6), 672–682 (2015).

[46]M. Salmanzadeh, G. Zahedi, G. Ahmadi, D. R. Marr, and M. Glauser, "Computational modeling of effects of thermal plume adjacent to the body on the indoor airflow and particle transport," J. Aerosol Sci. **53**, 29–39 (2012).

[47]B. A. Craven and G. S. Settles, "A computational and experimental investigation of the human thermal plume," J. Fluids Eng. **128**(6), 1251–1258 (2006).

[48]R. K. Bhagat, M. S. D. Wykes, S. B. Dalziel, and P. F. Linden, "Effects of ventilation on the indoor spread of COVID-19," J. Fluid Mech. **903**, F1 (2020).

[49]M. Roth, "Review of atmospheric turbulence over cities," Q. J. R. Meteorol. Soc. **126**(564), 941–990 (2000).

[50]O. G. Sutton, *Atmospheric Turbulence* (Routledge, 2020).

[51]L. Liu, Y. Li, P. V. Nielsen, J. Wei, and R. L. Jensen, "Short-range airborne transmission of expiratory droplets between two people," Indoor Air **27**(2), 452–462 (2017).

[52]S.-B. Kwon, J. Park, J. Jang, Y. Cho, D.-S. Park, C. Kim, G.-N. Bae, and A. Jang, "Study on the initial velocity distribution of exhaled air from coughing and speaking," Chemosphere **87**(11), 1260–1264 (2012).

[53]J. Wei and Y. Li, "Human cough as a two-stage jet and its role in particle transport," PLoS One **12**(1), e0169235 (2017).

[54]M. Abkarian, S. Mendez, N. Xue, F. Yang, and H. A. Stone, "Speech can produce jet-like transport relevant to asymptomatic spreading of virus," Proc. Natl. Acad. Sci. (published online 2020).

[55]O. V. Pyankov, S. A. Bodnev, O. G. Pyankova, and I. E. Agranovski, "Survival of aerosolized coronavirus in the ambient air," J. Aerosol Sci. **115**, 158–163 (2018).

[56]M. Schuit, S. Ratnesar-Shumate, J. Yolitz, G. Williams, W. Weaver, B. Green, D. Miller, M. Krause, S. Wood, B. Holland, J. Bohannon, D. Freeburger, I. Hooper, J. Biryukov, L. A. Altamura, V. Wahl, M. Hevey, and P. Dabisch, "Airborne SARS-CoV-2 is rapidly inactivated by simulated sunlight," J. Infect. Dis. **222**(4), 564–571 (2020).

[57]Evidence for Ultraviolet Radiation Decreasing COVID-19 Growth Rates: Global Estimates and Seasonal Implications.

[58]W. Yang, S. Elankumaran, and L. C. Marr, "Relationship between humidity and Influenza A viability in droplets and implications for influenza's seasonality," PLoS One **7**(10), e46789 (2012).

[59]The change in seasons may or may not affect the spread of COVID-19, National Academies http://sites.nationalacademies.org/BasedOnScience/change-in-seasons-may-or-may-not-affectthe-spread-of-COVID-19/index.htm; accessed July 31, 2020.

[60]S. Hallett, F. Toro, and J. V. Ashurst, "Physiology, tidal volume," in *StatPearls* (StatPearls Publishing, Treasure Island, FL, 2020).

[61]P. Santuz, E. Baraldi, M. Filippone, and F. Zacchello, "Exercise performance in children with asthma: Is it different from that of healthy controls?," Eur. Respir. J. **10**(6), 1254–1260 (1997).

[62]M. L. Aitken, J. L. Franklin, D. J. Pierson, and R. B. Schoene, "Influence of body size and gender on control of ventilation," J. Appl. Physiol. **60**(6), 1894–1899 (1986).

[63]E. P. Radford, "Ventilation standards for use in artificial respiration," J. Appl. Physiol. **7**(4), 451–460 (1955).

[64]P.-I. Lee, Y.-L. Hu, P.-Y. Chen, Y.-C. Huang, and P.-R. Hsueh, "Are children less susceptible to COVID-19?," J. Microbiol., Immunol. Infect. **53**(3), 371–372 (2020).

[65]D. A. Kass, P. Duggal, and O. Cingolani, "Obesity could shift severe COVID-19 disease to younger ages," Lancet **395**(10236), 1544–1545 (2020).

[66]N. Nikitin, E. Petrova, E. Trifonova, and O. Karpova, "Influenza virus aerosols in the air and their infectiousness," Adv. Virol. **2014**, 1.

[67]X. Tao, T. Garron, A. S. Agrawal, A. Algaissi, B.-H. Peng, M. Wakamiya, T.-S. Chan, L. Lu, L. Du, S. Jiang, R. B. Couch, and C.-T. K. Tseng, "Characterization and demonstration of the value of a lethal mouse model of middle east respiratory syndrome coronavirus infection and disease," J. Virol. **90**(1), 57–67 (2016).

[68]R. H. Alford, J. A. Kasel, P. J. Gerone, and V. Knight, "Human Influenza resulting from aerosol inhalation," Proc. Soc. Exp. Biol. Med. **122**(3), 800–804 (1966).

[69]M. Nicas, W. W. Nazaroff, and A. Hubbard, "Toward understanding the risk of secondary airborne infection: Emission of respirable pathogens," J. Occup. Environ. Hyg. **2**(3), 143–154 (2010).

[70]A. Konda, A. Prakash, G. A. Moss, M. Schmoldt, G. D. Grant, and S. Guha, "Aerosol filtration efficiency of common fabrics used in respiratory cloth masks," ACS Nano **14**, 6339 (2020).

[71]C. D. Zangmeister, J. G. Radney, E. P. Vicenzi, and J. L. Weaver, "Filtration efficiencies of nanoscale aerosol by cloth mask materials used to slow the spread of SARS-CoV-2," ACS Nano **14**(7), 9188–9200 (2020).

[72]N. H. L. Leung, D. K. W. Chu, E. Y. C. Shiu, K.-H. Chan, J. J. McDevitt, B. J. P. Hau, H.-L. Yen, Y. Li, D. K. M. Ip, J. S. M. Peiris, W.-H. Seto, G. M. Leung,

D. K. Milton, and B. J. Cowling, "Respiratory virus shedding in exhaled breath and efficacy of face masks," Nat. Med. **26**(5), 676–680 (2020).

[73]S. Verma, M. Dhanak, and J. Frankenfield, "Visualizing the effectiveness of face masks in obstructing respiratory jets," Phys. Fluids **32**(6), 061708 (2020).

[74]T. Dbouk and D. Drikakis, "On respiratory droplets and face masks," Phys. Fluids **32**(6), 063303 (2020).

[75]M.-R. Pendar and J. C. Páscoa, "Numerical modeling of the distribution of virus carrying saliva droplets during sneeze and cough," Phys. Fluids **32**(8), 083305 (2020).

[76]J. W. Tang, T. J. Liebner, B. A. Craven, and G. S. Settles, "A Schlieren optical study of the human cough with and without wearing masks for aerosol infection control," J. R. Soc., Interface **6**(Suppl. 6) (2009).

[77]L. Bourouiba, E. Dehandschoewercker, and J. W. M. Bush, "Violent expiratory events: On coughing and sneezing," J. Fluid Mech. **745**, 537–563 (2014).

[78]E. P. Fischer, M. C. Fischer, D. Grass, I. Henrion, W. S. Warren, and E. Westman, "Low-cost measurement of face mask efficacy for filtering expelled droplets during speech," Sci. Adv. **6**, eabd3083 (2020).

[79]J. F.-W. Chan, S. Yuan, A. J. Zhang, V. K.-M. Poon, C. C.-S. Chan, A. C.-Y. Lee, Z. Fan, C. Li, R. Liang, J. Cao, K. Tang, C. Luo, V. C.-C. Cheng, J.-P. Cai, H. Chu, K.-H. Chan, K. K.-W. To, S. Sridhar, and K.-Y. Yuen, "Surgical mask partition reduces the risk of noncontact transmission in a golden Syrian Hamster model for coronavirus disease 2019 (COVID-19)," Clin. Infect. Dis. (published online 2020).

[80]R. B. Bird, W. E. Stewart, and E. N. Lightfoot, *Transport Phenomena*, 2nd ed. (Wiley, 2006).

[81]H. Tennekes and J. L. Lumley, *A First Course in Turbulence* (MIT Press, 2018).

[82]G. A. Zarruk and E. A. Cowen, "Simultaneous velocity and passive scalar concentration measurements in low Reynolds number neutrally buoyant turbulent round jets," Exp. Fluids **44**(6), 865–872 (2008).

[83]F. Yang, A. A. Pahlavan, S. Mendez, M. Abkarian, and H. A. Stone, "Towards improved social distancing guidelines: Space and time dependence of virus transmission from speech-driven aerosol transport between two individuals," https://doi.org/medRxiv:2020.08.31.20185439.

[84]J. W. Tang, A. D. Nicolle, C. A. Klettner, J. Pantelic, L. Wang, A. B. Suhaimi, A. Y. L. Tan, G. W. X. Ong, R. Su, C. Sekhar, D. D. W. Cheong, and K. W. Tham, "Airflow dynamics of human jets: Sneezing and breathing—Potential sources of infectious aerosols," PLoS One **8**(4), e59970 (2013).

[85]R. I. Sykes and D. S. Henn, "Large-eddy simulation of concentration fluctuations in a dispersing plume," Atmos. Environ., Part A **26**(17), 3127–3144 (1992).

[86]I. Vinkovic, C. Aguirre, and S. Simoëns, "Large-eddy simulation and Lagrangian stochastic modeling of passive scalar dispersion in a turbulent boundary layer," J. Turbul. **7**, N30 (2006).

[87]W. Wu and U. Piomelli, "Reynolds-averaged and wall-modelled large-eddy simulations of impinging jets with embedded azimuthal vortices," Eur. J. Mech. B/Fluids **55**, 348–359 (2016).

[88]K. Norton, L. Norton, and D. Sadgrove, "Position statement on physical activity and exercise intensity terminology," J. Sci. Med. Sport **13**(5), 496–502 (2010).

[89]G. Valli, M. Internullo, A. M. Ferrazza, P. Onorati, A. Cogo, and P. Palange, "Minute ventilation and heart rate relationship for estimation of the ventilatory compensation point at high altitude: A pilot study," Extreme Physiol. Med. **2**, 7 (2013).

[90]G. N. Sze To and C. Y. H. Chao, "Review and comparison between the Wells–Riley and dose-response approaches to risk assessment of infectious respiratory diseases," Indoor Air **20**(1), 2–16 (2010).

[91]G. N. Sze To, M. P. Wan, C. Y. H. Chao, F. Wei, S. C. T. Yu, and J. K. C. Kwan, "A methodology for estimating airborne virus exposures in indoor environments using the spatial distribution of expiratory aerosols and virus viability characteristics," Indoor Air **18**(5), 425–438 (2008).

[92]M. Gandhi, C. Beyrer, and E. Goosby, "Masks do more than protect others during COVID-19: Reducing the inoculum of SARS-CoV-2 to protect the wearer," J. Gen. Intern. Med. (2020).

[93]W. Feller, *An Introduction to Probability Theory and its Applications* (Wiley, 1991), Vol. 2.

[94]C. J. Noakes, C. B. Beggs, P. A. Sleigh, and K. G. Kerr, "Modelling the transmission of airborne infections in enclosed spaces," Epidemiol. Infect. **134**(5), 1082–1091 (2006).

[95]R. O. J. H. Stutt, R. Retkute, M. Bradley, C. A. Gilligan, and J. Colvin, "A modelling framework to assess the likely effectiveness of facemasks in combination with 'lock-down' in managing the COVID-19 pandemic," Proc. R. Soc. A **476**(2238), 20200376 (2020).

[96]T. Watanabe, T. A. Bartrand, M. H. Weir, T. Omura, and C. N. Haas, "Development of a dose-response model for SARS coronavirus," Risk Anal. **30**(7), 1129–1138 (2010).

[97]J. Ferry and S. Balachandar, "A fast Eulerian method for disperse two-phase flow," Int. J. Multiphase Flow **27**(7), 1199–1226 (2001).

[98]A. K. Aiyer, D. Yang, M. Chamecki, and C. Meneveau, "A population balance model for large eddy simulation of polydisperse droplet evolution," J. Fluid Mech. **878**, 700–739 (2019).

[99]D. Yang, B. Chen, S. A. Socolofsky, M. Chamecki, and C. Meneveau, "Large-eddy simulation and parameterization of buoyant plume dynamics in stratified flow," J. Fluid Mech. **794**, 798–833 (2016).

[100]M. Germano, U. Piomelli, P. Moin, and W. H. Cabot, "A dynamic subgrid-scale eddy viscosity model," Phys. Fluids A **3**(7), 1760–1765 (1991).

[101]C. Meneveau, T. S. Lund, and W. H. Cabot, "A Lagrangian dynamic subgrid-scale model of turbulence," J. Fluid Mech. **319**, 353–385 (1996).

[102]C. Scalo, L. Boegman, and U. Piomelli, "Large-eddy simulation and low-order modeling of sediment-oxygen uptake in a transitional oscillatory flow," J. Geophys. Res.: Oceans **118**(4), 1926–1939, https://doi.org/10.1002/jgrc.20113 (2013).

[103]A quote attributed to Howard Skipper, an American doctor.